# Leader–Follower Formation Control of Multiple Non-holonomic Mobile Robots Incorporating a Receding-horizon Scheme


**Jian Chen**
Laboratory for Mechatronics and Controls,
Joint Advanced Research Institute,
City University of Hong Kong,
Hong Kong,
People's Republic of China
and
University of Science and Technology of China,
Suzhou,
People's Republic of China
lixiang@mail.ustc.edu.cn

**Dong Sun**
Department of Manufacturing Engineering
and Engineering Management,
City University of Hong Kong
Hong Kong,
People's Republic of China
medsun@cityu.edu.hk

**Jie Yang**
Department of Precision Machinery and Instrumentations,
University of Science and Technology of China,
Hefei,
People's Republic of China
jieyang@ustc.edu.cn

**Haoyao Chen**
Laboratory for Mechatronics and Controls,
Joint Advanced Research Institute,
City University of Hong Kong,
Hong Kong,
People's Republic of China
And
University of Science and Technology of China,
Suzhou,
People's Republic of China
hychen5@mail.ustc.edu.cn



## Abstract

*In this paper we present a receding-horizon leader–follower (RH-LF) control framework to solve the formation problem of multiple non-holonomic mobile robots with a rapid error convergence rate. To maintain the desired leader–follower relationship, we propose a separation–bearing–orientation scheme (SBOS) for two-robot formations and separation–separation–orientation scheme (SSOS) for three-robot formations in deriving the desired postures of the followers. Unlike the other leader–follower approaches in the existing literature, the orientation deviations between the leaders and followers are explicitly controlled in our framework, which enables us to successfully solve formation controls when robots move backwards, which is termed as a formation backwards problem in this paper. Further, we propose to incorporate the receding-horizon scheme into our leader–follower controller to yield a fast convergence rate of the formation tracking errors. Experiments are finally performed on a group*



The International Journal of Robotics Research
Vol. 29, No. 6, May 2010, pp. 727–747
DOI: 10.1177/0278364909104290



Figures 6, 8–10, 12–14, 16–18 appear in color online: http://ijr.sagepub.com

*of mobile robots to demonstrate the effectiveness of the proposed formation control framework.*

KEY WORDS—multiple mobile robots, formation, leader–follower, receding horizon.

## 1. Introduction

Coordination of multiple mobile robots has received considerable attention over the past decade. It is well known that multiple mobile robots, if working cooperatively under highly efficient organizations and principles, can behave like a whole, with fault tolerance and robust properties (Liu and Wu 2001). A robot team can perform tasks that are difficult for one single robot. Some examples are group hunting (Yamaguchi 1999; Cao et al. 2006), large area exploration (Burgard et al. 2005), surveillance (Tang and Ozguner 2005), object transportation (Yamashita et al. 2003; Berman et al. 2004), and spacecraft interferometry tasks (Beard et al. 2001).

Robot formation control has received much attention in multi-robot coordination in recent years. Several formation control approaches have been proposed in the literature, such as behavior-based methods, leader–follower methods and virtual structure methods, to name a few. In the behavior-based formation, a group behavior (or mission) comprises some low-level actions (or sub-tasks) and is constructed to achieve the global objective, where the individual robot needs to perform low-level actions to accomplish the group behavior (Balch and Arkin 1998; Parker 1998; Lawton et al. 2003; Berman et al. 2004; Long et al. 2005). In the leader–follower formation, one robot is designated as the leader, whose motion defines the group bulk motion, and the other robots are controlled to follow their respective leaders with given separations and bearings (Desai et al. 2001; Das et al. 2002; Tanner et al. 2003, 2004; Takahashi et al. 2004; Huang et al. 2006). In the virtual structure formation, robots behave like particles embedded in a rigid virtual structure (Lewis and Tan 1997; Egerstedt and Hu 2001; Ren and Beard 2004). Some other methods were proposed based on artificial potentials (Ogren et al. 2001; Sepulchre et al. 2007) and graph theory (Jadbabaie et al. 2003; Fax and Murray 2004; Olfati-Saber and Murray 2004; Moreau 2005; Olfati-Saber 2006). A novel formation approach was recently developed by Gu (2008), where the formation task is formulated as a linear-quadratic Nash differential game through the use of graph theories. Sun and Wang (2007); Wang and Sun (2008) transferred the formation problem to a synchronization control problem, and a synchronous controller was developed to converge both the position and synchronization (formation) errors toward zero in formation switching tasks.

The receding-horizon (RH) method, which is also known as model predictive control (MPC), aims to solve optimization problems of a predictive control horizon with input and state constraints (Keerthi and Gilbert 1988). A major concern in the use of a predictive horizon is that whether such an open-loop control can guarantee system stability. It was shown that an infinitive predictive control horizon could guarantee stability of a system (Keerthi and Gilbert 1988), but the infinitive predictive horizon may not be feasible for a non-linear system in practice. The stability could also be ensured by adding a terminal state constraint to the system, e.g., driving the terminal state to zero (Rawlings and Muske 1993), but this approach was time consuming (Gu and Hu 2005). Further research showed that within the terminal state region, the system was stable if the terminal state penalty function was larger than the cost function of the linear feedback controller (Chen and Allgower 1998; De Nicolao et al. 1998). Recent works have suggested that the feedback controller in the terminal state region was not necessarily linear, and therefore the assumption that the optimal control must be continuous was no longer needed (Fontes 2001). It was a conclusion that the system could be stable as long as the combination of the cost function and the first derivative of the terminal state penalty function are less than or equal to zero, which provided an opportunity to the receding horizon control in solving the non-holonomic point-wise stabilization problems (Fontes 2001; Gu and Hu 2005).

In this paper, we propose a new leader–follower control framework to control a group of non-holonomic mobile robots in formation tasks and, furthermore, we incorporate the RH method into the leader–follower strategy to achieve a fast convergence rate for the whole formation control framework. We perform this research mainly in the following two perspectives.

First, we study the new leader–follower control framework with consideration of separation, bearing and orientation derivations between leaders and followers together. With an assumption that all separation, bearing and orientation deviations are enumerated in advance, we propose two control schemes, the *separation–bearing–orientation scheme* (SBOS) and *separation–separation–orientation scheme* (*SSOS*), for two-robot and three-robot formations, respectively. Desai et al. (2001) and Das et al. (2002) investigated the leader–follower formation problem with graph theory, and proposed two basic leader–follower schemes: separation–bearing control (SBC) and separation–separation control (SSC). The major difference between our schemes and those of Desai et al. (2001) and Das et al. (2002) is that the orientation will be explicitly controlled in SBOS and SSOS, while in SBC and SSC the orientation between the leaders and followers were controlled implicitly using feedback linearization, based on a defined reference frame. Use of explicit control of orientation in SBOS and SSOS helps us to achieve more effective formation activities of a multi-robot group. For example, many existing leader–follower methods could not address the formation problem when the robots move backwards together, which is termed

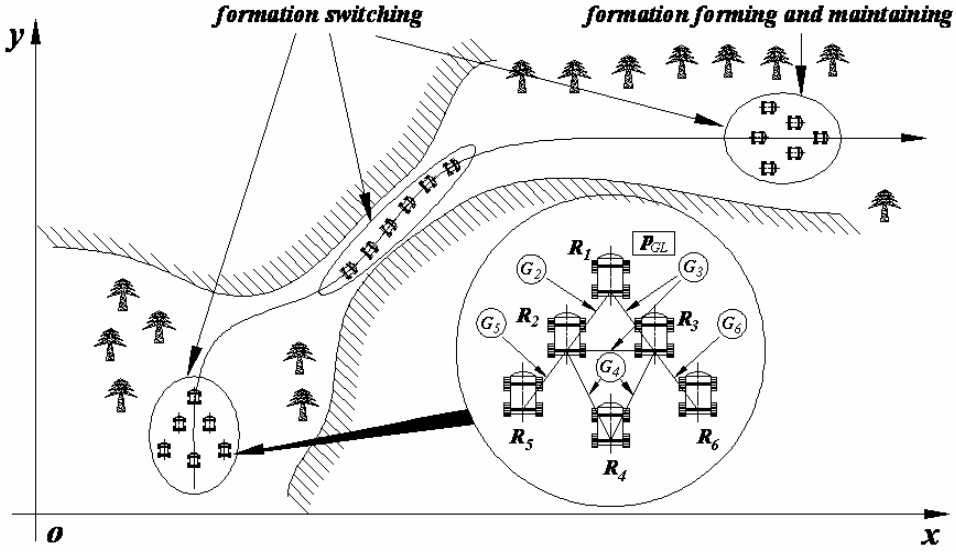


Fig. 1. Trajectory tracking of a group of robots accompanied by formation forming, maintaining and switching.

as the "formation backwards problem" in this paper. Using our new leader–follower framework, this formation backwards problem can be solved successfully owing to the addition of an explicit orientation control to the robots.

Second, we incorporate the RH strategy to the leader–follower approach to improve the convergence rate of the defined formation tracking errors. The rapid converging speed of the robot state is critical since it has a direct effect on the overall formation performance of the whole group. Through proper design of the RH procedure, we propose a so-called receding-horizon leader–follower (RH-LF) control scheme to yield exponential convergence of the robots' formation tracking errors in the terminal state region. Note that most formation controls in the existing literature were investigated based on stability analysis only, and few of them were based on stability as well as performance optimization to achieve fast convergence.

The paper is organized as follows. In Section 2, the RH-LF formation control framework will be presented, which includes the generation of the robots' desired postures based on the required leader–follower relationships, robot motion controller considering the non-holonomic constraint, and incorporation of the RH scheme to the robot controller. Experiments on a group of three mobile robots are reported in Section 3 to verify the effectiveness of the proposed approach. Finally, conclusions of this work are given in Section 4.

For more localization methods concerning multiple mobile robot group, the readers are suggested to refer to Chen (2009) and the references there in.

## 2. RH-LF Formation Control Framework

### *2.1. Formation Control Problem*

Consider that a group of non-holonomic mobile robots move along a desired trajectory while meeting various formation requirements such as formation forming, maintaining and switching. Figure 1 illustrates an example where a group of six robots moves along a desired trajectory as a whole. During the motion, the robots are required to maintain a triangular formation first, then switch to a sequential formation to pass through the valley, and finally switch back and maintain the triangular formation. With the leader–follower formation strategy, the group leader $R_1$, whose configuration is defined as $p_{GL}$, leads the group bulk motion, and the other robots, labeled as $R_i$ with index $i = 2, 3, \ldots, n$, where $n$ is the total number of robots in the group, are the followers that maintain the respective relationships with the group leader $R_1$. A number of leader–follower pairs are introduced with pre-defined relationships of $G_2, G_3, \ldots, G_n$, where $G_i = LF\left(R_j \leftarrow R_i\right)$ or $G_i = LF\left(\left(R_j, R_k\right) \leftarrow R_i\right)$ with $(j, k) < i$, and $R_j$, $R_k$ are the leaders and $R_i$ the follower. As seen in Figure 1, one follower may follow one leader or two leaders in the formation. To design the relationship $G_i$, two physically close robots are determined as two neighbors for easy sensorial connection. All robots in the group are linked, either directly or indirectly, as a network in the group movement. The robots are labeled in advance based on their relative positions in the group at the beginning. Without loss of generality, we assume that the desired formation configurations are designed in a feasible way such that the robots can form the required formations without conflicts with each other.

Formation protocols for coordinating and organizing the grouped robots to accomplish the formation task is an interesting topic and has been studied extensively, e.g., by Desai et al. (2001) and Das et al. (2002), to name a few. In this paper, we focus our attention on the formation control only. The problem to be investigated is formulated as follows: a group of $n$ non-holonomic mobile robots are controlled to move along a desired trajectory, led by the group leader $R_1$, whose configuration determines the bulk motion of the group; the remaining robots $R_2 - R_n$ are controlled to follow the leader $R_1$ with the required leader–follower relationships $G_2 - G_n$, through controlling separation, bearing and orientation deviation of the followers with respect to the leaders.

Consider that the robots are differential mobile robots with non-holonomic constraints. The robot posture, denoted by $p_i = \begin{bmatrix} x_i & y_i & \theta_i \end{bmatrix}^{\mathrm{T}}$, is described by a unicycle model as the follows

$$\dot{p}_i = \begin{bmatrix} \dot{x}_i \\ \dot{y}_i \\ \dot{\theta}_i \end{bmatrix} = \begin{bmatrix} \cos\theta_i \\ \sin\theta_i \\ 0 \end{bmatrix} v_i + \begin{bmatrix} 0 \\ 0 \\ 1 \end{bmatrix} \omega_i, \qquad (1)$$

where $x_i$ and $y_i$ are robot coordinates in the $x$–$y$ plane, $\theta_i$ is the heading angle (or orientation) of the robot, and $v_i$ and $\omega_i$ are the linear and angular velocities of the robot.

In the following, we propose a new leader–follower framework to address the formation control problem of non-holonomic mobile robots as defined above. The framework will contain generation of the desired postures of the followers based on the required leader–follower relationships, motion control design with consideration of robots' non-holonomic constraints, and the incorporation of the receding-horizon scheme to the robot controller to yield fast convergence rate on the formation tracking errors.

### *2.2. Generation of the desired postures of followers*

To ensure the followers maintain the desired separation, bearing and orientation deviation with respect to the leaders, we propose two control schemes to derive the desired postures of the followers. The two schemes are *SBOS* for two-robot formations and *SSOS* for three-robot formations.

#### *2.2.1. SBOS*

Consider a two-robot formation with the desired leader–follower relationship $G_i = LF\left(R_j \leftarrow R_i\right)$, as shown in Figure 2. Under the leader–follower scheme SBOS, $R_i$ follows $R_j$ with desired separation $l^d_{i,j}$, bearing $\psi^d_{i,j}$ and orientation deviation $\beta^d_{i,j}$. The desired posture $p^d_i = \begin{bmatrix} x^d_i & y^d_i & \theta^d_i \end{bmatrix}^{\mathrm{T}}$ of the follower $R_i$ is then given by

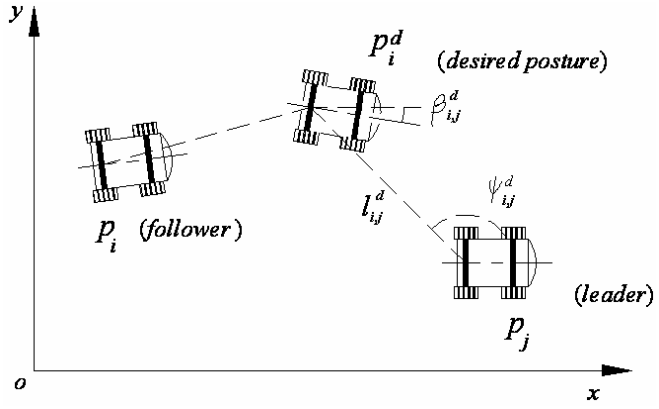


Fig. 2. Two-robot formation with SBOS.

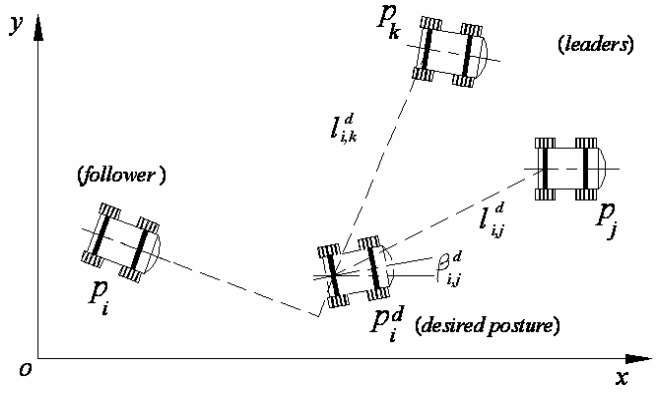


Fig. 3. Three-robot formation with SSOS.

$$p^d_i = \begin{bmatrix} x^d_i \\ y^d_i \\ \theta^d_i \end{bmatrix} = \begin{bmatrix} x_j + l^d_{i,j}\cos\psi^d_{i,j} \\ y_j + l^d_{i,j}\sin\psi^d_{i,j} \\ \theta_j + \beta^d_{i,j} \end{bmatrix}. \qquad (2)$$

#### *2.2.2. SSOS*

Consider a three-robot formation as shown in Figure 3, where $G_i = LF\left(\left(R_j, R_k\right) \leftarrow R_i\right)$. Under the leader–follower scheme SSOS, $R_i$ is required to maintain desired separations $l^d_{i,j}$ and $l^d_{i,k}$ with respect to $R_j$ and $R_k$, respectively, and meanwhile to maintain a desired orientation deviation $\beta^d_{i,j}$ with respect to $R_j$. The desired posture for the follower $R_i$ can be determined by

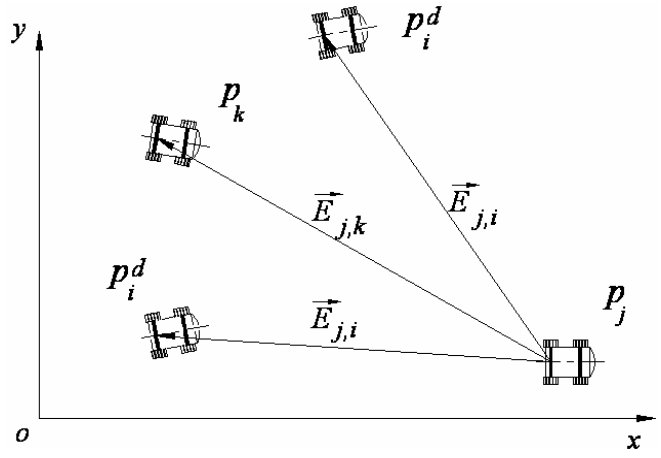


Fig. 4. Follower reference configuration with SSOS.

$$p_i^d = \begin{bmatrix} x_i^d \\ y_i^d \\ \theta_i^d \end{bmatrix} = \begin{bmatrix} \left(b_i \pm \left(b_i^2 - 4a_i c_i\right)\right)/a_i \\ \left(M_i - \Delta x_i x_i^d\right)/\Delta y_i \\ \theta_j + \beta_{i,j}^d \end{bmatrix}, \quad (3)$$

where $M_i = \frac{1}{2}\left[\left(x_j^2 - x_k^2\right) + \left(y_j^2 - y_k^2\right) - \left(l_{i,j}^d\right)^2 + \left(l_{i,k}^d\right)^2\right]$, $\Delta x_i = x_j - x_k$, $\Delta y_i = y_j - y_k$, and

$$\begin{bmatrix} a_i \\ b_i \\ c_i \end{bmatrix} = \begin{bmatrix} 2\left(\Delta x_i^2 + \Delta y_i^2\right) \\ 2\left(M_i \Delta x_i - \Delta y_i\left(\Delta x_i y_j - \Delta y_i x_j\right)\right) \\ \left(M_i - \Delta y_i y_j\right)^2 - \left(\Delta y_i x_j\right)^2 - \left(\Delta y_i l_{i,j}^d\right)^2 \end{bmatrix}.$$

The detailed derivation of (3) is given in the appendix. Note that the desired posture in (3) requires the use of both $l_{i,j}^d$ and $l_{i,k}^d$. To derive the unique solution of $p_i^d$ from (3), we need to compare directions of the two vectors $\vec{E}_{j,i}$ and $\vec{E}_{j,k}$, as shown in Figure 4, which are defined as

$$\begin{cases} \vec{E}_{j,i} = \left(\left(x_i^d - x_j\right), \left(y_i^d - y_j\right)\right) \\ \vec{E}_{j,k} = \left(\left(x_k - x_j\right), \left(y_k - y_j\right)\right) \end{cases}.$$

These give a criterion of

$$N = \left(x_i^d - x_j\right)\left(y_k - y_j\right) - \left(x_k - x_j\right)\left(y_i^d - y_j\right). \quad (4)$$

When $R_i^d$ is at the left-hand side of $\vec{E}_{j,k}$, select $x_i^d$ from the two possible solutions in (3) such that $N > 0$. (Only one solution of $x_i^d$ in (3) leads to $N > 0$.) When $R_i^d$ is at the right-hand side of $\vec{E}_{j,k}$, determine $x_i^d$ such that $N < 0$.

Note that with the above SSOS, the follower must follow two leaders with two desired separations simultaneously. This implicitly requires that the two leaders must be well configured and controlled in the leader–follower formation. Otherwise, the follower may encounter difficulty in simultaneously maintaining the required separations to the two leaders.

### 2.3. Robot Control

The robot control aims to drive the robot $R_i$ toward its desired posture $p_i^d = [x_i^d \quad y_i^d \quad \theta_i^d]^{\mathrm{T}}$ such that the desired leader–follower relationship can be achieved. Define the posture error of the robot $R_i$ as $p_i^e = p_i^d - p_i$. In a similar manner to Kanayama et al. (1990), we transfer the posture error $p_i^e$, by multiplying a rotation matrix about $\theta_i$, to a new error $e_i$, which is defined as the formation tracking error in this paper, i.e.

$$e_i = \begin{bmatrix} e_{x,i} \\ e_{y,i} \\ e_{\theta,i} \end{bmatrix} = \begin{bmatrix} \cos\theta_i & \sin\theta_i & 0 \\ -\sin\theta_i & \cos\theta_i & 0 \\ 0 & 0 & 1 \end{bmatrix} p_i^e = T_i p_i^e. \quad (5)$$

Since $T_i$ in (5) is invertible, $e_i \to 0$ implies $p_i^e \to 0$. Our next control goal is to drive the formation tracking error $e_i$ to zero. Differentiating (5) with respect to time, and then submitting (1) into the resulting equation and utilizing the non-holonomic constraint of $\dot{x}_i \sin\theta_i - \dot{y}_i \cos\theta_i = 0$, we have the following error dynamics (Kanayama et al. 1990)

$$\dot{e}_i = \begin{bmatrix} \dot{e}_{x,i} \\ \dot{e}_{y,i} \\ \dot{e}_{\theta,i} \end{bmatrix} = \begin{bmatrix} v_i^d \cos e_{\theta,i} \\ v_i^d \sin e_{\theta,i} \\ \omega_i^d \end{bmatrix} + \begin{bmatrix} -1 \\ 0 \\ 0 \end{bmatrix} v_i + \begin{bmatrix} e_{y,i} \\ -e_{x,i} \\ -1 \end{bmatrix} \omega_i, \quad (6)$$

where $v_i^d$ and $\omega_i^d$ are the desired translational and rotary velocities of the robot $R_i$, which can be derived by differentiating $p_i^d$. In the following, we discuss how to drive $e_i$ towards zero.

In a similar manner to Jiang and Nijmeijer (1997), a controller used to stabilize the error dynamics (6) is presented as

$$\begin{bmatrix} v_i \\ \omega_i \end{bmatrix} = \begin{bmatrix} v_i^d \cos e_{\theta,i} + k_{x,i} e_{x,i} \\ \omega_i^d + k_{\theta,i} e_{\theta,i} + v_i^d e_{y,i} \dfrac{\sin e_{\theta,i}}{e_{\theta,i}} \end{bmatrix}, \quad (7)$$

where $k_{x,i}$ and $k_{\theta,i}$ are positive control gains, and $\sin e_{\theta,i}/e_{\theta,i} \to 1$ when $e_{\theta,i} \to 0$.

Substituting (7) into (6) yields the following closed-loop dynamics

$$\dot{e}_i = \begin{bmatrix} \dot{e}_{x,i} \\ \dot{e}_{y,i} \\ \dot{e}_{\theta,i} \end{bmatrix} = \begin{bmatrix} -k_{x,i} e_{x,i} + e_{y,i} \omega_i \\ v_i^d \sin e_{\theta,i} - e_{x,i} \omega_i \\ -k_{\theta,i} e_{\theta,i} - v_i^d e_{y,i} \sin\left(e_{\theta,i}\right) / e_{\theta,i} \end{bmatrix}. \quad (8)$$

**Proposition 1.** *Assume that $v_i^d$ and $\omega_i^d$ are uniformly continuous and bounded in $t \in [0, \infty)$. The formation tracking error $e_i$ is globally and uniformly bounded. Further, if $v_i^d$ does not converge to zero in tracking, $e_i$ asymptotically converges to zero, i.e. $e_i \to 0$ as $t \to \infty$.*

**Proof:** Consider a Lyapunov function candidate as

$$V(e_i) = \frac{1}{2}\left(e_{x,i}^2 + e_{y,i}^2 + e_{\theta,i}^2\right). \quad (9)$$

Taking the time derivative of $V(e_i)$ and utilizing (8), we have

$$\begin{aligned} \dot{V}(e_i) &= e_{x,i}\dot{e}_{x,i} + e_{y,i}\dot{e}_{y,i} + e_{\theta,i}\dot{e}_{\theta,i} \\ &= -k_{x,i} e_{x,i}^2 - k_{\theta,i} e_{\theta,i}^2 \le 0. \end{aligned} \quad (10)$$

Therefore, $V(e_i)$ is non-increasing for all $e_i$. Since $e_{x,i}$ and $e_{\theta,i}$ appear in (10), they are bounded in terms of $L_2$ norm. Since $e_{y,i}$ is further bounded from (9), we have $\dot{e}_{x,i}$ and $\dot{e}_{\theta,i}$ are bounded from the closed loop dynamics (8). Hence, $e_{x,i}$ and $e_{\theta,i}$ are uniformly continuous. From Barbalat's lemma, we have $e_{x,i} \to 0$ and $e_{\theta,i} \to 0$ as time $t \to \infty$.

When $e_{x,i} = 0$ and $e_{\theta,i} = 0$, we have the following result from (8)

$$\dot{e}_{\theta,i} = -v_i^d e_{y,i} = 0. \quad (11)$$

If $v_i^d$ does not converge to zero, we have $e_{y,i} = 0$ from (11). Therefore, the invariant set of the closed-loop dynamics (8) in the set $\left\{(e_i, \dot{e}_i) : \dot{V}(e_i) = 0\right\}$ contains zero error, i.e. $e_i = 0$. Using LaSalle's theorem, we finally conclude that $e_i \to 0$ as time $t \to \infty$. □

A traditional way to implement the controller (7) is to select constant control gains $k_{x,i} > 0$ and $k_{\theta,i} > 0$. Use of constant control gains can guarantee the system stability, but may not achieve the goal of optimization. In the following, we incorporate the RH scheme into the controller (7) to optimize the control gains $k_{x,i}$ and $k_{\theta,i}$, such that a fast convergence rate of the error $e_i$ can be achieved.

### *2.4. RH Control Scheme*

We now discuss how to incorporate the RH scheme into the robot controller (7) to improve the convergence speed. The general RH control procedure was presented by Fontes (2001).

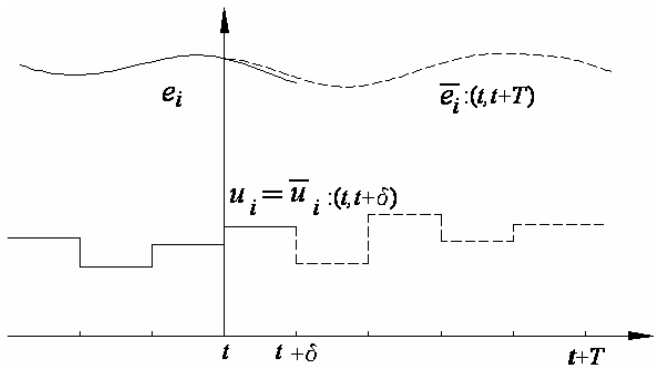


Fig. 5. General RH scheme.

Define $u_i(t) = [v_i(t) \quad \omega_i(t)]^{\mathrm{T}}$ as the two-dimensional input to the robot $R_i$. Rewrite (8) as a nominal non-linear plant expressed as follows:

$$\dot{e}_i(t) = f(e_i(t), u_i(t)). \quad (12)$$

The RH scheme is performed with steps as shown in Figure 5, where $\delta$ and $T$ denote the sampling time period and the predictive horizon length, respectively. Here $\bar{u}_i : (t, t+T)$ and $\bar{e}_i : (t, t+T)$ are the computed input vector and the predicted error state during the predictive horizon. Note that when applying an input vector to the plant over the time period $(t, t+T)$, the error $e_i$ during $(t, t+T)$ can be predicted by $\dot{e}_i(\tau) = f(e_i(\tau), u_i(\tau))$, where $\tau \in (t, t+T)$. The procedures of a general RH scheme are listed as follows.

(1) Measure the error state $e_i$ at time instant $t$.

(2) Compute an input sequence $\bar{u}_i : (t, t+T)$ along the predictive horizon. Following (12), the generated predictive error state sequence $\bar{e}_i : (t, t+T)$ from $\bar{u}_i : (t, t+T)$ should contain the terminal error state $\bar{e}_i(t+T)$ that falls in the required terminal state region.

(3) Apply $u_i = \bar{u}_i$ to the robot in the time interval $(t, t+\delta)$, and the remaining $\bar{u}_i : (t+\delta, t+T)$ is discarded.

(4) Repeat steps (1) to (3) at the next time instant $t_{\text{next}} = t + \delta$.

Generally speaking, the RH scheme aims to minimize the sum of a terminal state penalty function $g(e_i(t+T))$ and a running cost function $L(e_i(t), u_i(t))$ measured during the predictive horizon $(t, t+T)$. The terminal state penalty function should be continuous, differentiable, and positive-definite if $e_i(t+T) \neq 0$, which can be represented as

$$\begin{aligned} g(e_i(t+T)) &= \frac{1}{2}\left(e_{x,i}^2(t+T) + e_{y,i}^2(t+T)\right. \\ &+ \left. e_{\theta,i}^2(t+T)\right). \end{aligned} \quad (13)$$

The running cost function $L(e_i(t), u_i(t))$ is defined as

$$L(e_i(t), u_i(t)) = e_i(t)^T Q e_i(t) + u_i(t)^T R u_i(t), \quad (14)$$

where $Q > 0$ and $R \geq 0$ are the symmetric weight matrices.

**Proposition 2:** *Choose the terminal state penalty function $g(e_i(t+T))$ as (13). Choose the running cost function with*

$$Q = \begin{bmatrix} q_{x,i} & & \\ & q_{y,i} & \\ & & q_{\theta,i} \end{bmatrix} \quad \text{and} \quad R = 0$$

to yield

$$L(e_i(t), u_i(t)) = q_{x,i} e_{x,i}^2(t) + q_{y,i} e_{y,i}^2(t) + q_{\theta,i} e_{\theta,i}^2(t), \quad (15)$$

*where $q_{x,i}$, $q_{y,i}$ and $q_{\theta,i}$ are positive constant weight parameters. Define the terminal state region $\Omega$ as*

$$\begin{aligned} \Omega = \{ & (k_{x,i}(t), k_{\theta,i}(t)) \,|\, k_{x,i}(t) \geq q_{x,i}, \\ & k_{\theta,i}(t) \geq q_{\theta,i}, e_{y,i}(t+T) = 0 \}. \end{aligned} \quad (16)$$

*Then the errors $e_{x,i}$ and $e_{\theta,i}$ exponentially converge to zero in the terminal state region $\Omega$, with an exponential rate of $k_{x,i}(t)$ and $k_{\theta,i}(t)$, respectively.*

**Proof:** Fontes (2001) and Gu and Hu (2005) proved that the RH stability can be guaranteed in the terminal state region if the following condition is satisfied

$$\dot{g}(e_i(t)) + L(e_i(t), u_i(t)) \leq 0. \quad (17)$$

Substituting (8) into (17) and considering that the control gains $k_{x,i}$ and $k_{\theta,i}$ are time-varying, yields

$$\begin{aligned} & \dot{g}(e_i(t)) + L(e_i(t), u_i(t)) \\ = \; & e_{x,i}\dot{e}_{x,i} + e_{y,i}\dot{e}_{y,i} + e_{\theta,i}\dot{e}_{\theta,i} + q_{x,i}e_{x,i}^2 \\ + \; & q_{y,i}e_{y,i}^2 + q_{\theta,i}e_{\theta,i}^2 \\ = \; & -(k_{x,i}(t) - q_{x,i})e_{x,i}^2 - (k_{\theta,i}(t) - q_{\theta,i})e_{\theta,i}^2 + q_{y,i}e_{y,i}^2. \end{aligned} \quad (18)$$

In the terminal state region $\Omega$ as given in (16), $e_{y,i} = 0$. We then have $\dot{g}(e_i(t)) + L(e_i(t), u_i(t)) \leq 0$ from (16) and (18), which confirms the stability when using the RH scheme to determine the control gains.

From (8), we further have the following dynamics in the terminal state region

$$\begin{bmatrix} \dot{e}_{x,i}(t) \\ \dot{e}_{\theta,i}(t) \end{bmatrix} = - \begin{bmatrix} k_{x,i}(t) e_{x,i}(t) \\ k_{\theta,i}(t) e_{\theta,i}(t) \end{bmatrix}. \quad (19)$$

Since $k_{x,i}(t) > 0$ and $k_{\theta,i}(t) > 0$, Equation (19) implies that $e_{x,i}$ and $e_{\theta,i}$ are exponentially convergent to zero, with an exponential rate of $k_{x,i}(t)$ and $k_{\theta,i}(t)$, respectively. □

**Remark:** Proposition 2 holds only in the terminal state region $\Omega$. Therefore, $e_{y,i} \to 0$ must be achieved first by using the standard RH control scheme. This can be done through a trial of the control gains $k_{x,i}$ and $k_{\theta,i}$ in using the controller (7) at time instant $t$ to predict the system outputs at time instant $t+T$, and then applying the gains that can yield $e_{y,i} \to 0$ to the controller. When the robot state enters the terminal state region $\Omega$ (namely $e_{y,i}$ towards zero), Equation (19) shows that $e_{x,i}$ and $e_{\theta,i}$ exponentially converge to zero without prediction on them. This implies that the time-consuming RH scheme is used only for driving $e_{y,i}$ to zero, and there is no need to apply it for $e_{x,i}$ and $e_{\theta,i}$. Therefore, the computational cost is saved.

## 3. Experiments

### *3.1. Experiment Setup*

Experiments were performed on a group of three mobile robots supplied by *ActiveMedia Robotics* to verify the feasibility and effectiveness of the proposed RH-LF formation control strategy. The three robots were one *Amigo* robot which was designated as the leader $R_1$, and two *P3-DX Pioneer* robots which were designated as the followers $R_2$ and $R_3$. The experiments were carried out in the indoor environment.

The *Amigo* robot (the leader) is equipped with a 44.2368 MHz Renesas SH2 32-bit RISC microprocessor, which receives remote control signals and generates the velocity inputs for the robot motion control. The *P3-DX Pioneer* robots (the followers) employ a control architecture with two levels: one onboard PC for communication and programming, and one 44.2368 MHz Renesas SH2 32-bit RISC microprocessor for robot motion control. The robots and a central computer-controlled workstation communicate with each other via a 54.0 MHz wireless access point.

A camera installed on ceiling of the laboratory is used to capture images. The images are transmitted to the workstation for processes of posture initialization and rectification. The posture information is obtained by the encoders equipped on the robots. After refreshing the configuration information of the robots, the server distributes the posture information and the required leader–follower relationships to the embedded computer of the *P3-DX* follower. The server has four threads running in parallel to communicate with the image processing workstation and the two *P3-DX Pioneer* robots, and to control the *Amigo* leader directly. These four threads share the same

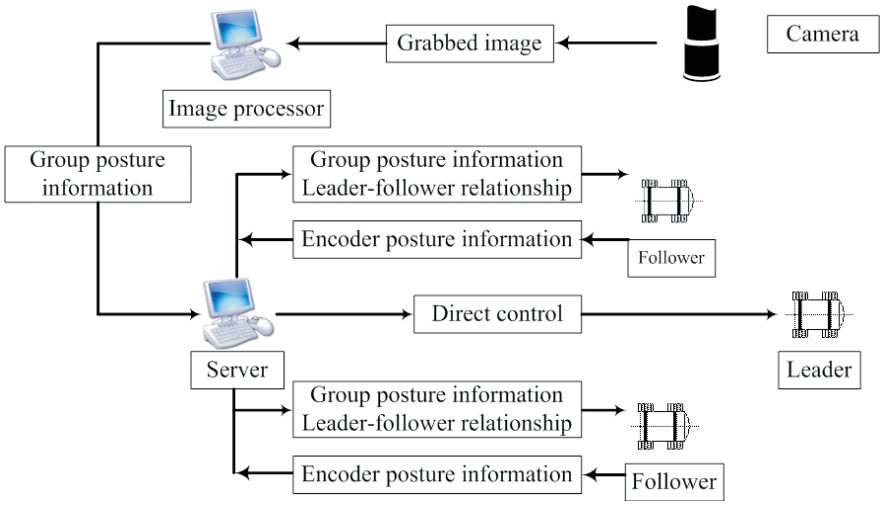


Fig. 6. Overall control architecture.

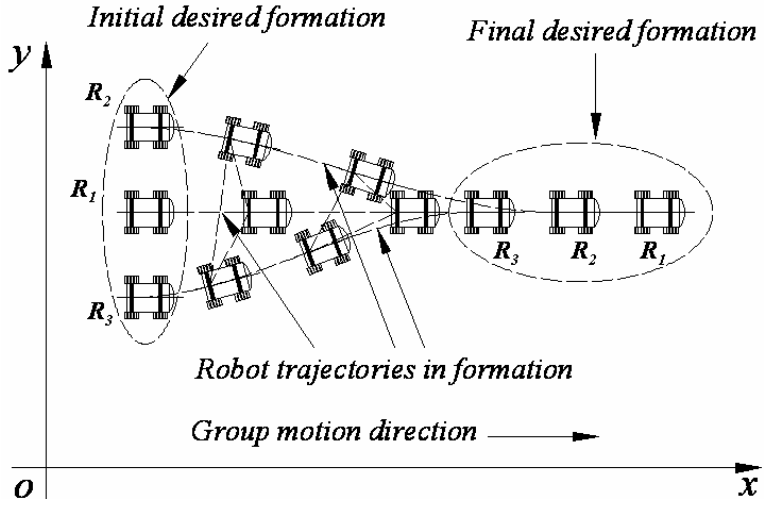


Fig. 7. Three robots in formation tracking.

memory in which the robots' postures and the leader–follower relationships are stored. The four threads are controlled by one mutex lock to avoid data confusion.

There are two threads in the embedded computer of each *P3-DX* robot. One is for data communication with the server and the other for running the control algorithm. After receiving the group posture information, *PC-104* generates the linear and angular velocity inputs based on the proposed RH-LF formation controller, and sends the inputs to the *LM296* motor control units. The overall control architecture is shown in Figure 6.

### *3.2. Experiment Results*

Experiments were performed on the robot group to test the proposed formation control strategy, for solving the problem of robot trajectory tracking while accompanied by formation forming, maintenance and switching.

The first experiment was to control the three robots in a switching task from a collateral formation to a sequential formation when following individual desired trajectory, as shown in Figure 7. At the beginning of the experiment, the robots were placed with the initial configurations of $R_1(0.5\ \text{m}, 1.5\ \text{m}, 0)$, $R_2(0\ \text{m}, 2.5\ \text{m}, -90^o)$ and

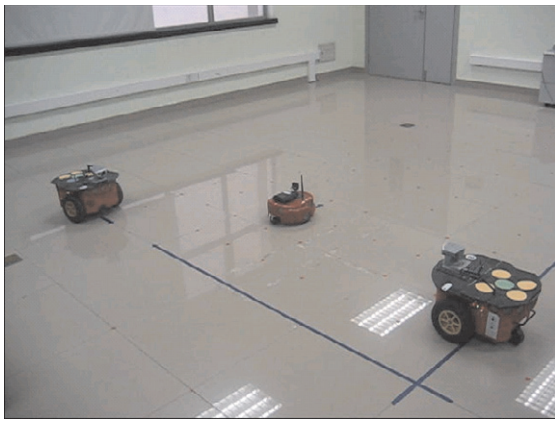

(a) Beginning

(b) After 7 seconds

(c) After 16 seconds

(d) After 23 seconds

(e) After 29 seconds

(f) After 45 seconds

Fig. 8. Taped video images of the robot group formation.

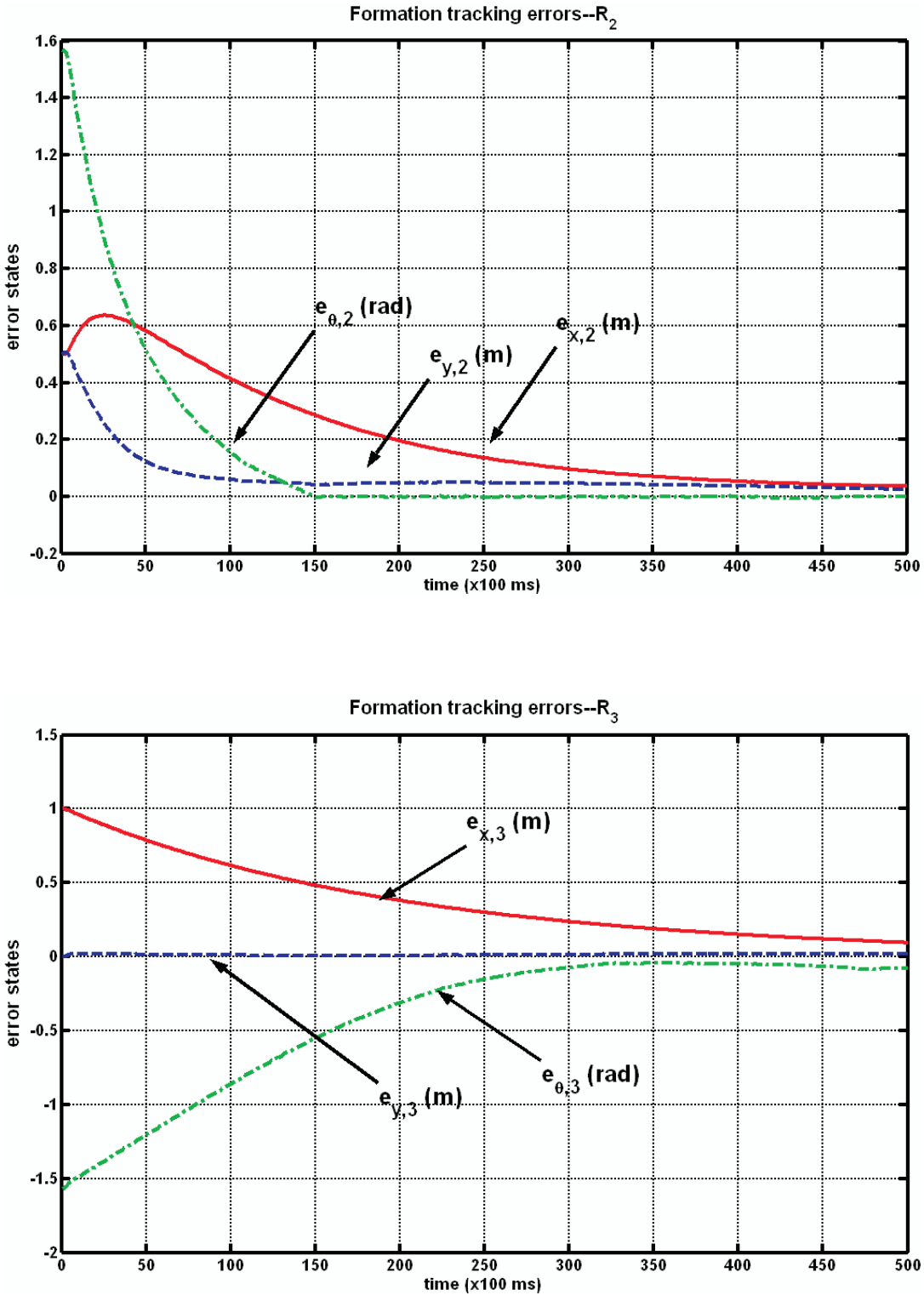


Fig. 9. Formation tracking errors of the followers.

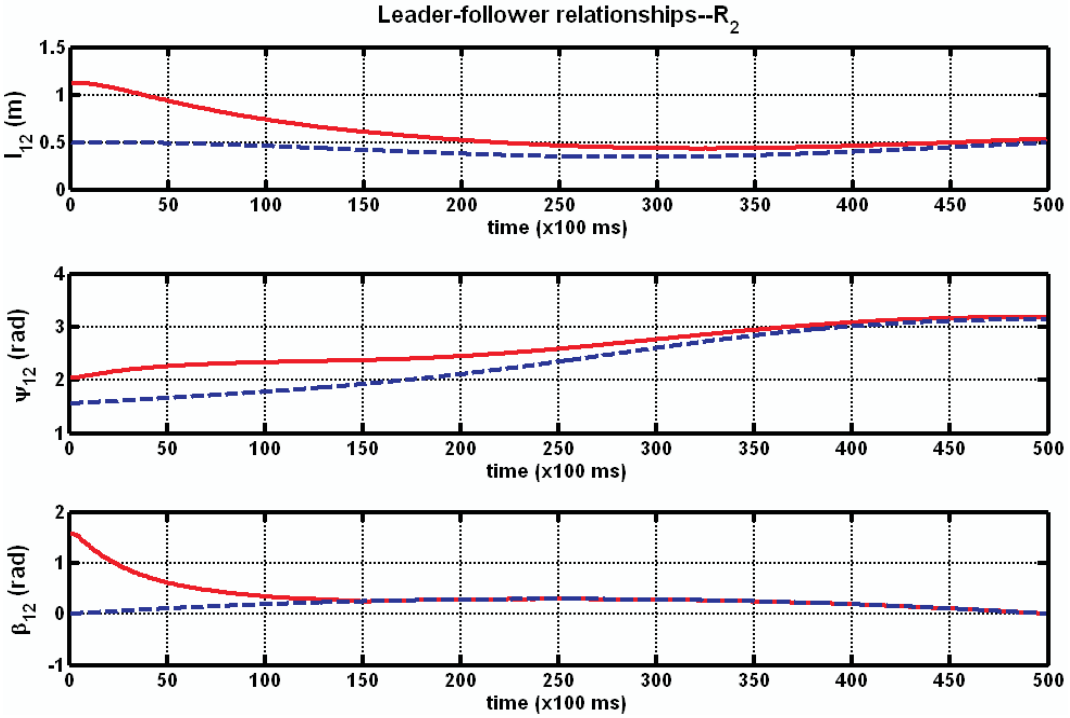


(a)

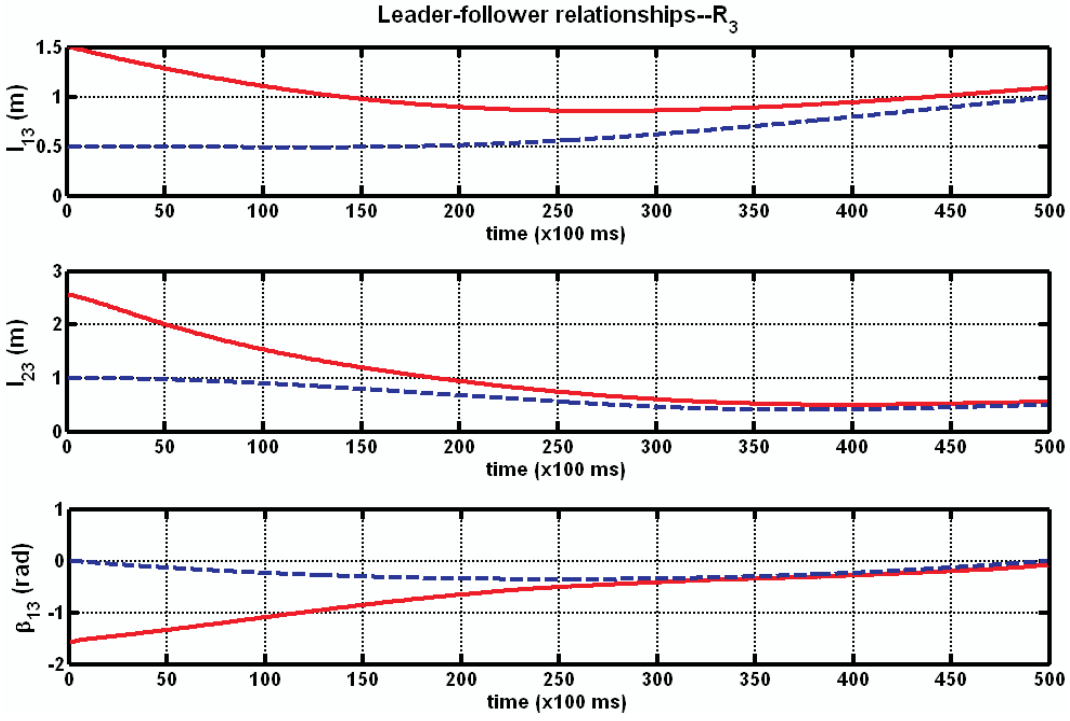


(b)

Fig. 10. Leader–follower formation relationships. (Solid line: Actual. Dashed line: Desired.)

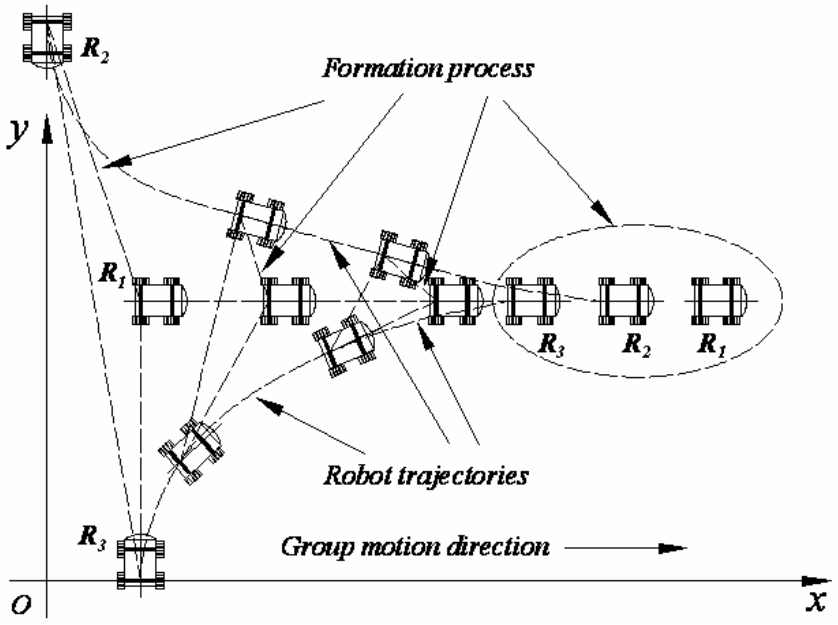


Fig. 11. Actual tracking of robots with formation.

$R_3(0.5\text{ m}, 0\text{ m}, 90^\circ)$. The controller (7) with fixed constant control gains were applied first, which was followed by the use of the same controller but with time-varying control gains through incorporation of the RH scheme, to demonstrate improved convergence. In the experiment, the sampling time period was 100 ms, and the constant feedback control gains without applying the RH scheme were chosen as $k_{x,i} = 0.1\ \text{s}^{-1}$ and $k_{\theta,i} = 0.3\ \text{s}^{-1}$ $(i = 2, 3)$, determined by a trial-and-error method.

Figure 8 illustrates the formation process collected from the video. Figure 8(a) shows the robot group at the beginning, and Figures 8(b)–(f) show the robot group at different times. In these figures, the two long lines define the $x$ and $y$ coordinate axes, and the three arrowed short lines point the initial postures of the robots. The small *Amigo* robot $R_1$ leads the two *P3-DX* followers $R_2$ and $R_3$ to follow the desired trajectory. $R_2$ was controlled to follow $R_1$ by the SBOS, and $R_3$ was controlled to follow $R_1$ and $R_2$ by the SSOS.

Figure 9 shows the formation tracking errors of the followers $R_2$ and $R_3$. Figure 10 shows the leader–follower relationships, including separation $l_{12}$, bearing $\psi_{12}$ and orientation deviation $\beta_{12}$ between $R_1$ and $R_2$ in Figure 10(a), and separation $l_{12}$ between $R_1$ and $R_3$, separation $l_{23}$ between $R_2$ and $R_3$ and orientation deviation $\beta_{13}$ between $R_1$ and $R_3$ in Figure 10(b). These results demonstrate the good performance of both position tracking and formation controls. Figure 11 illustrates the real robot group formation.

We then incorporated the RH scheme into the controller (7) to verify the effectiveness of the proposed RH-LF strategy. The weight parameters were set as $q_{x,i} = q_{y,i} = q_{\theta,i} = 0.01$ $(i = 2, 3)$, for both followers. The predictive horizon was chosen as $T = 1$ s. Figure 12 illustrates the formation tracking errors of the two followers. Compared with the results in Figure 9, the error convergence speed is much increased. Figure 13 illustrates values of the applied feedback control gains in RH scheme, where $k_{x,i}$ was predicted from 0.01 to 0.5 $\text{s}^{-1}$ and $k_{\theta,i}$ was predicted from 0.01 to 0.3 $\text{s}^{-1}$ for both followers. As seen in Figures 12 and 13, the error $e_{y,i}$ of both followers $R_2$ and $R_3$ entered the terminal state region $\Omega$ at about 5 seconds. Figure 14 illustrates the leader–follower relationships with the proposed RH-LF controller. Figure 14(a) illustrates separation $l_{12}$, bearing $\psi_{12}$ and orientation deviation $\beta_{12}$ between $R_1$ and $R_2$. Figure 14(b) illustrates separation $l_{13}$ between $R_1$ and $R_3$, separation $l_{23}$ between $R_2$ and $R_3$, and orientation deviation $\beta_{13}$ between $R_1$ and $R_3$. All of these results display much improved converging performance when compared with that in Figure 10.

Furthermore, we carried out the experiment in a formation backwards task utilizing the proposed RH-LF controller. The three robots were placed with initial configurations of $R_1(5\text{ m}, 1\text{ m}, 0^\circ)$, $R_2(6.5\text{ m}, 2\text{ m}, 0^\circ)$ and $R_3(7\text{ m}, 0\text{ m}, 0^\circ)$. The same parameters of the RH-LF controller were chosen. Results are shown in Figure 15, where both $R_2$ and $R_3$ were controlled by SBOS to follow $R_1$. The formation tracking errors of the two followers $R_2$ and $R_3$ are shown in Figure 16. Figure 17 illustrates the applied control gains. Figure 18 illustrates the leader–follower relationships including separation $l_{12}$, bearing $\psi_{12}$, and orientation deviation $\beta_{12}$ between $R_1$ and

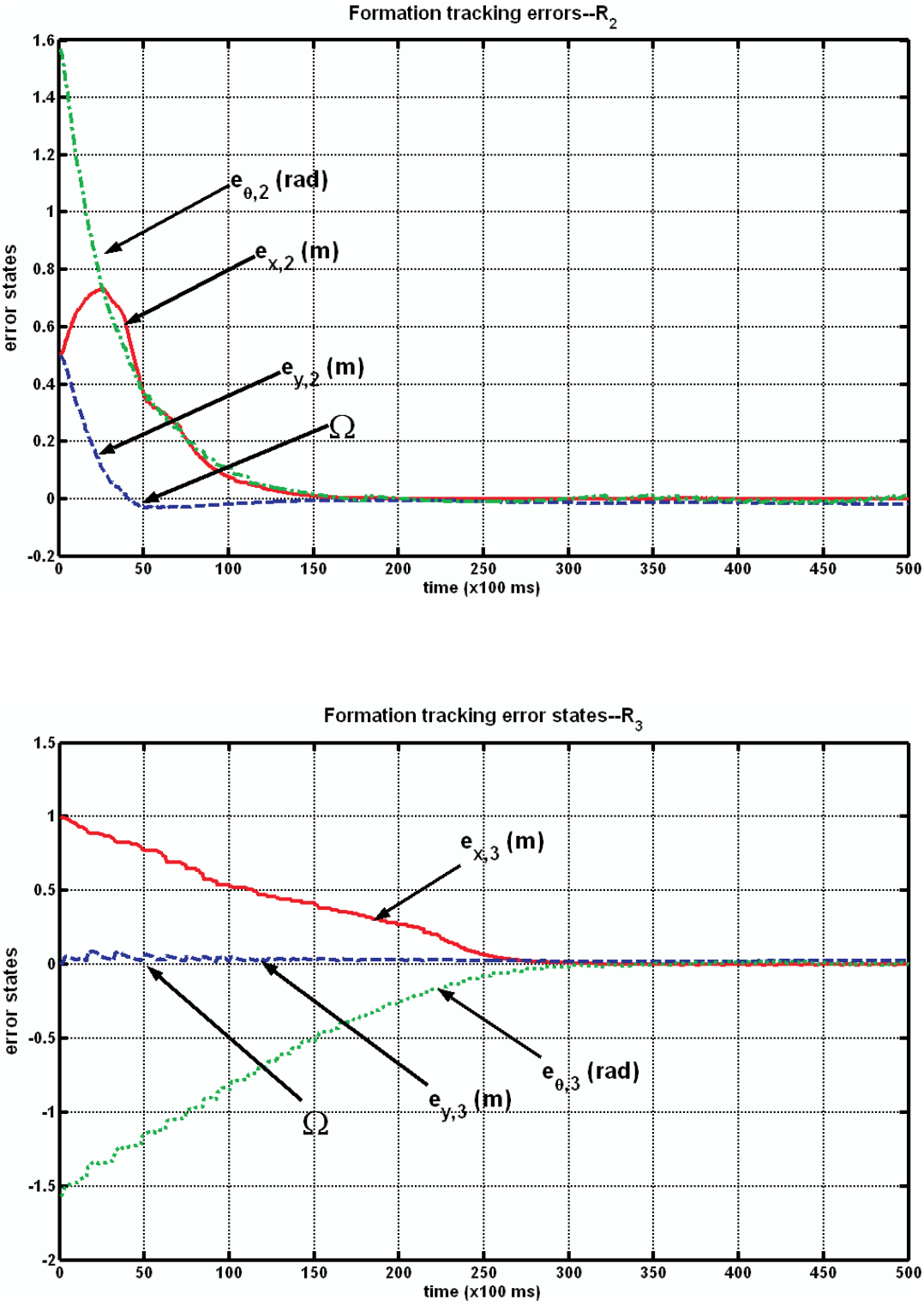


Fig. 12. RH-LF formation tracking errors of the followers.

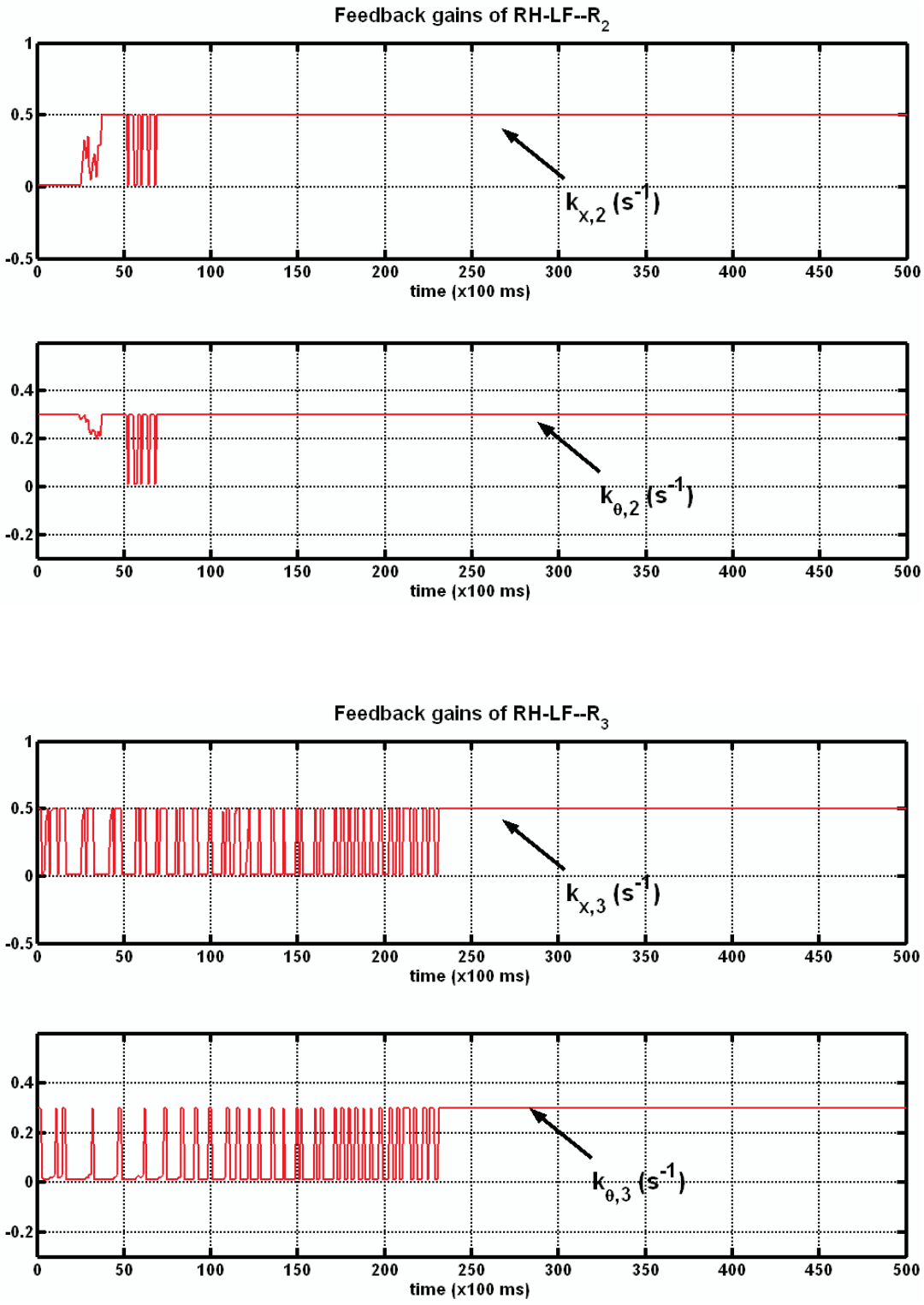


Fig. 13. Feedback gains of RH-LF for the followers.

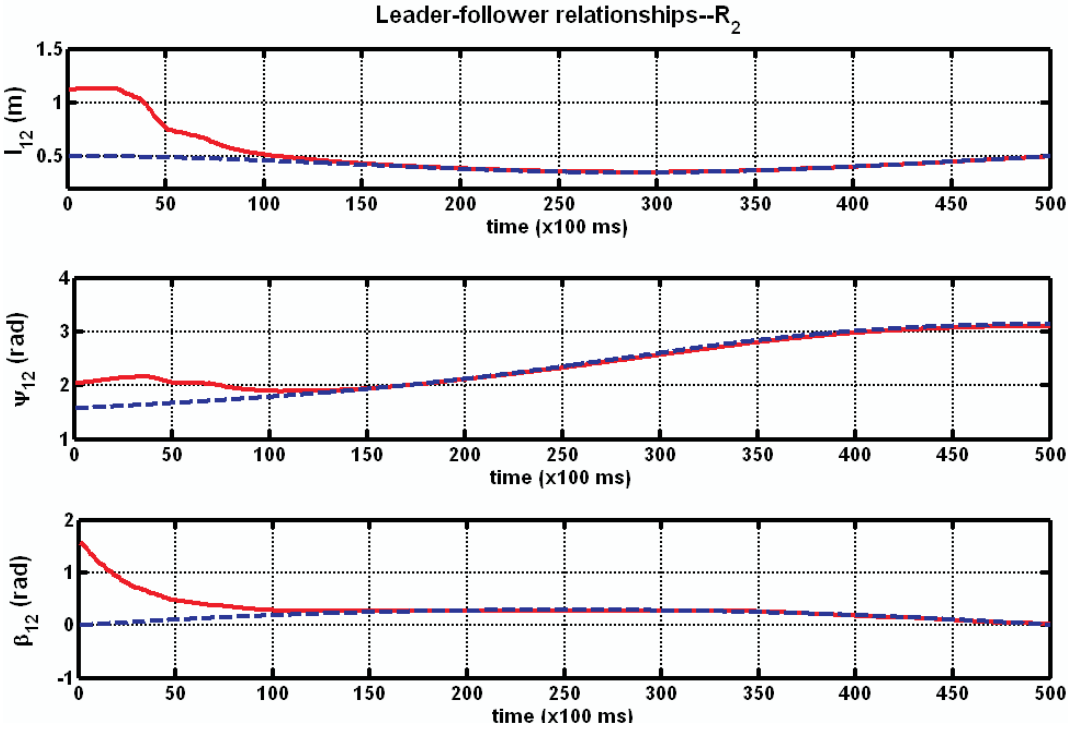


(a)

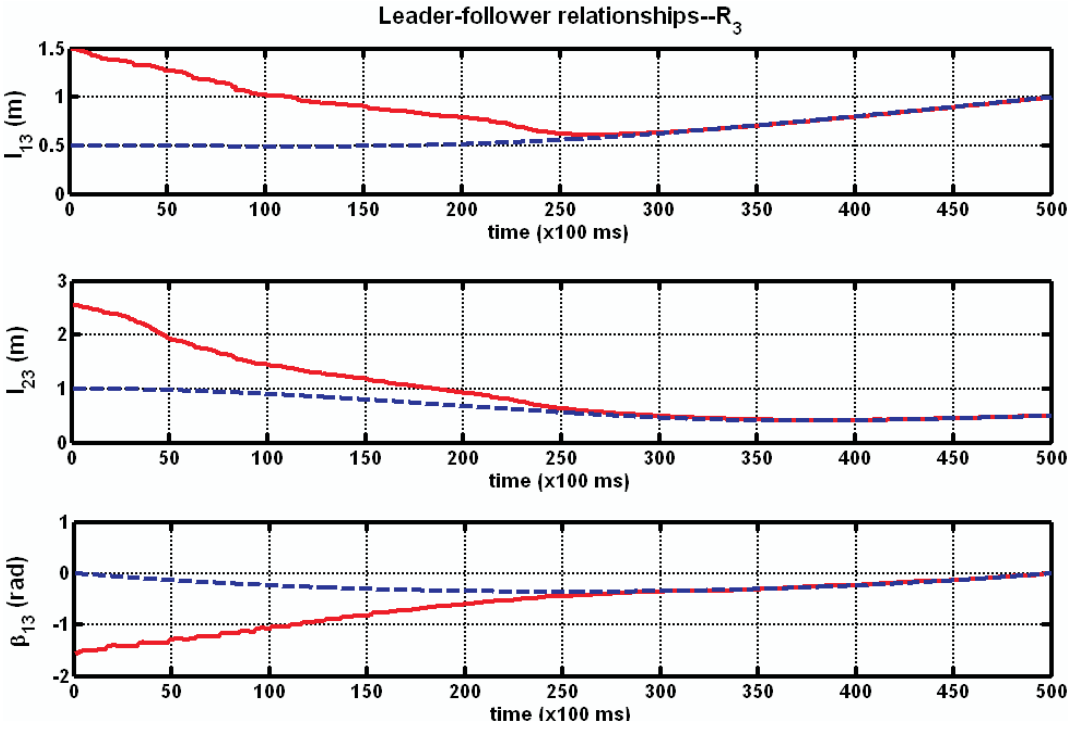


(b)

Fig. 14. RH-LF leader–follower formation relationships. (Solid: Actual. Dashed: Required, RH-LF.)

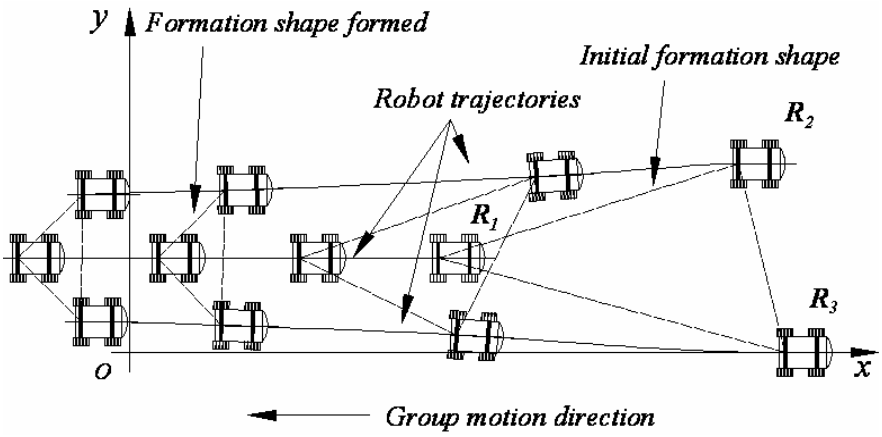


Fig. 15. Robots moving backwards with formation when applying RH-LF.

$R_2$ in Figure 18(a), and separation $l_{13}$, bearing $\psi_{13}$, and orientation deviation $\beta_{13}$ between $R_1$ and $R_3$ in Figure 18(b). These results verify that the proposed RH-LF scheme can effectively control the robots when moving backwards with formation.

## 4. Conclusions

In this paper we have presented a RH-LF control scheme for multiple non-holonomic mobile robots engaged in formation tasks. A new formation control framework has been developed for controlling separation, bearing and orientation deviation between leaders and followers together. Two control schemes, *SBOS* and *SSOS* developed for two-robot and three-robot formations, respectively, have been utilized to generate the desired robot postures based on the formation requirement. A robot motion controller is designed to stabilize the formation tracking errors, with consideration of robot non-holonomic constraints. The RH control scheme is incorporated into the robot controller to achieve exponential convergence of the formation tracking errors. Experiments are performed on a group of three mobile robots, to demonstrate effectiveness of the proposed RH-LF formation controller. Future works include an investigation of applying the RH-LF approach to solve obstacle avoidance problems in clustered environment, and the research on the group dynamical topology and task assignment problems.

## Acknowledgements

This work was supported in part by a grant from Research Grants Council of the Hong Kong Special Administrative Region, China under grant CityU 119907, and a grant from City University of Hong Kong under project 7002461.

## Appendix

The following equations were obtained with the desired separations and orientation deviation between the follower $R_i$ and its leaders $R_j$ and $R_k$

$$\begin{cases} \left(x_j - x_i^d\right)^2 + \left(y_j - y_i^d\right)^2 = \left(l_{i,j}^d\right)^2 \\ \left(x_k - x_i^d\right)^2 + \left(y_k - y_i^d\right)^2 = \left(l_{i,k}^d\right)^2 \\ \beta_i^d = \beta_j + \beta_{i,j}^d \end{cases} \tag{20}$$

where $l_{i,j}^d$ is the desired separation between $R_i$ and $R_j$, $l_{i,k}^d$ is the desired separation between $R_i$ and $R_k$, and $\beta_{i,j}^d$ is the desired orientation deviation between $R_i$ and $R_j$.

Substituting the first equation of (20) into the second equation of (20) and following the definitions in (3), we have

$$\Delta x_i x_i^d + \Delta y_i y_i^d = M. \tag{21}$$

Substituting (21) into the first equation of (20) yields

$$\frac{1}{2} a_i \left(x_i^d\right)^2 - b_i x_i^d + c_i = 0. \tag{22}$$

Solving (21) yields the solution

$$x_i^d = \left(b_i \pm \left(b_i^2 - 4a_i c_i\right)\right)/a_i. \tag{23}$$

Substituting $x_i^d$ into (21) yields

$$y_i^d = \left(M_i - \Delta x_i x_i^d\right)/\Delta y_i. \tag{24}$$

Finally, we have

$$p_i^d = \begin{bmatrix} x_i^d \\ y_i^d \\ \theta_i^d \end{bmatrix} = \begin{bmatrix} \left(b_i \pm \left(b_i^2 - 4a_i c_i\right)\right)/a_i \\ \left(M_i - \Delta x_i x_i^d\right)/\Delta y_i \\ \theta_j + \beta_{i,j}^d \end{bmatrix}. \tag{25}$$

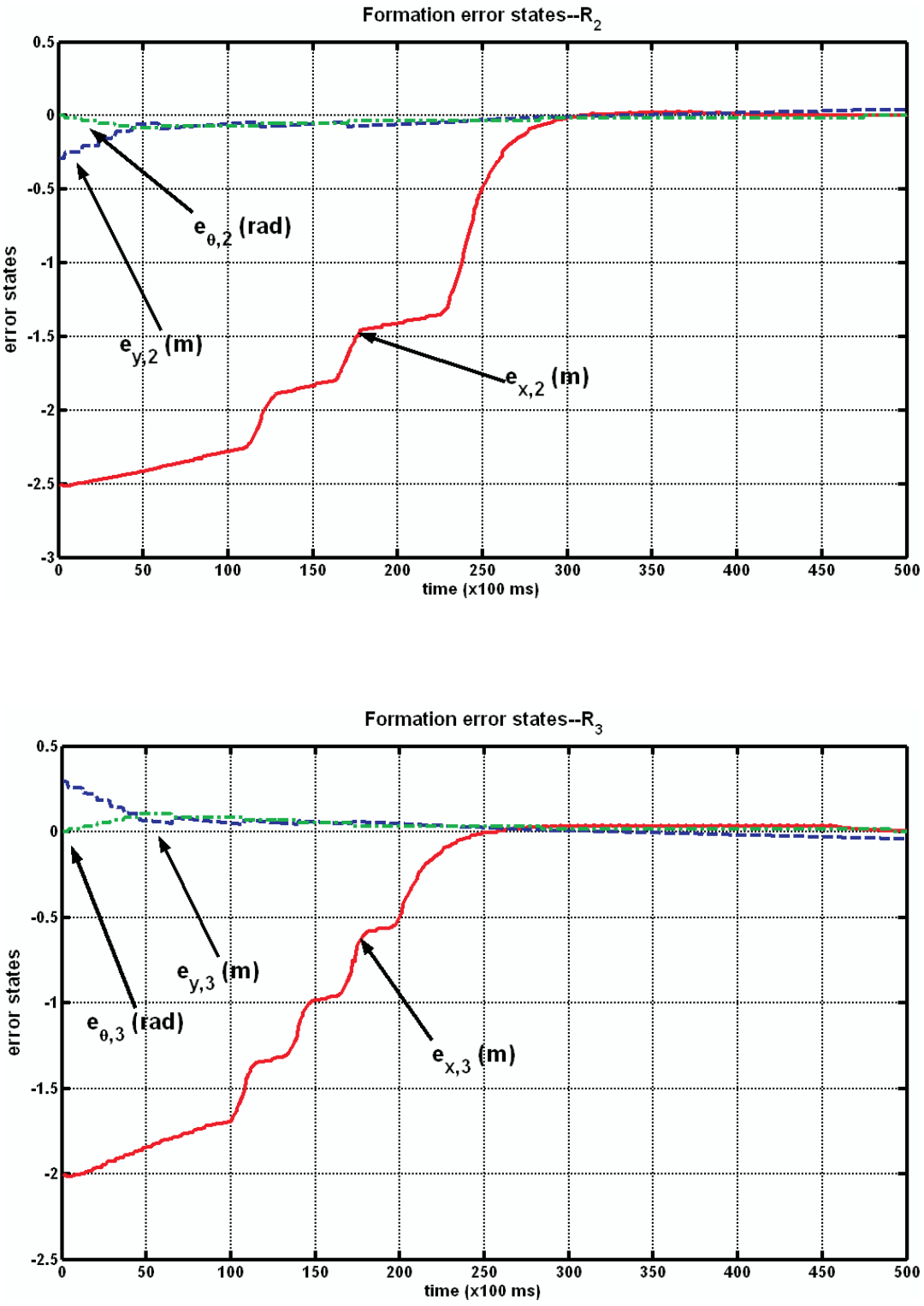


Fig. 16. Formation tracking errors of the followers in the formation backwards task.

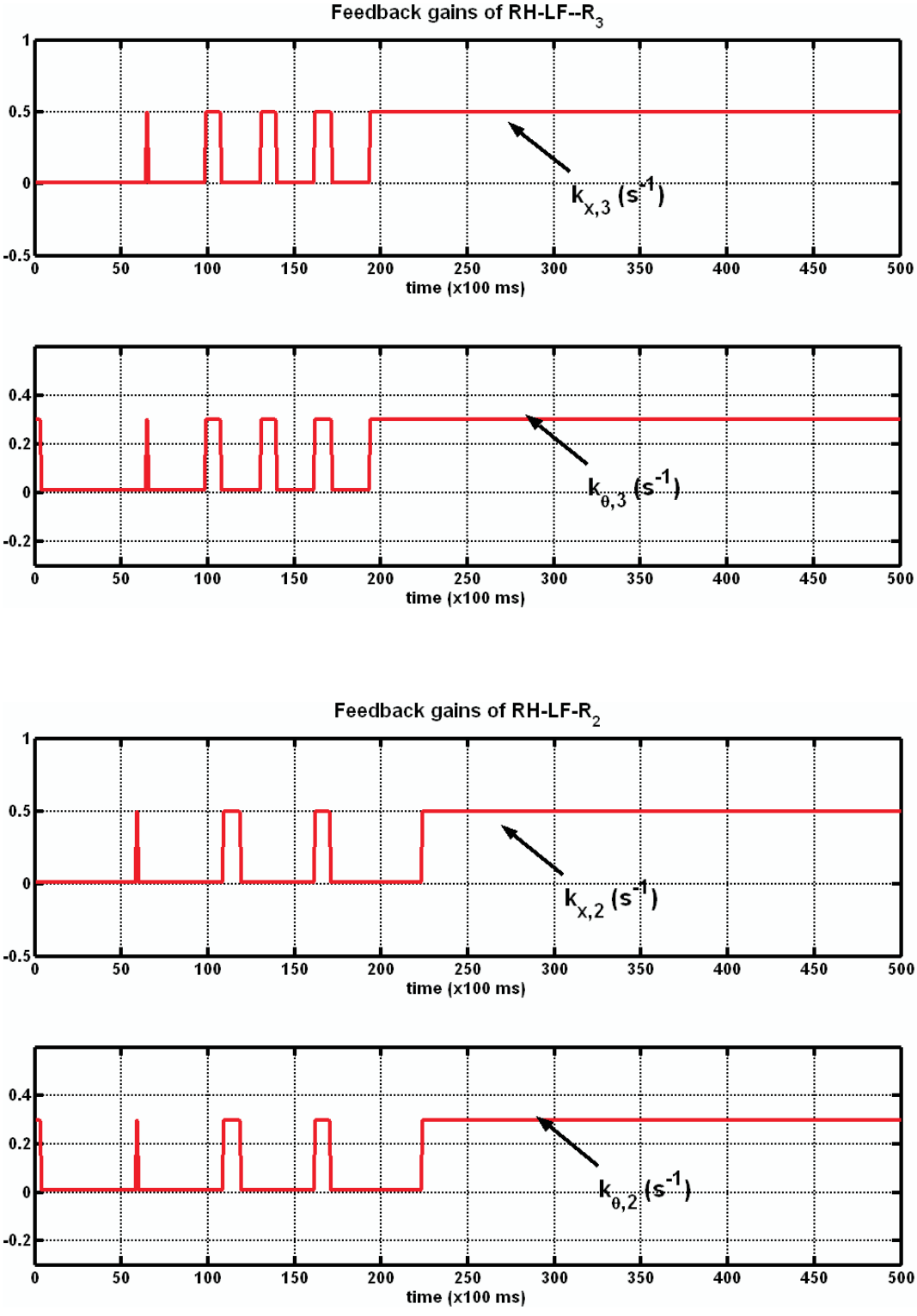


Fig. 17. RH-LF control gains of the followers.

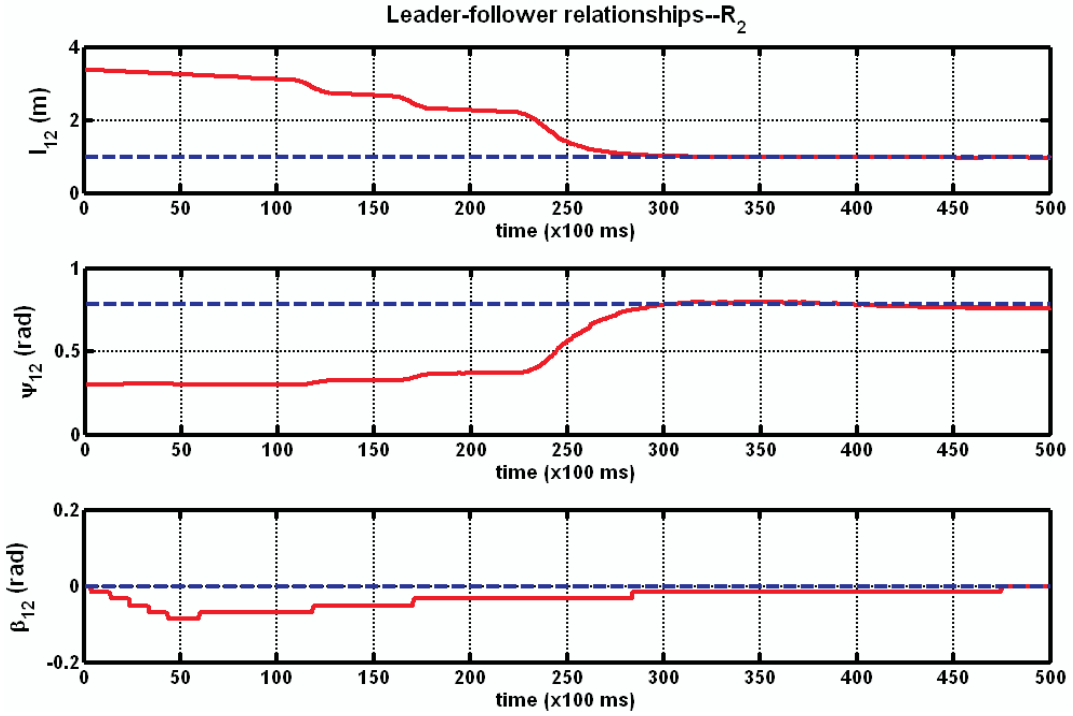


(a)

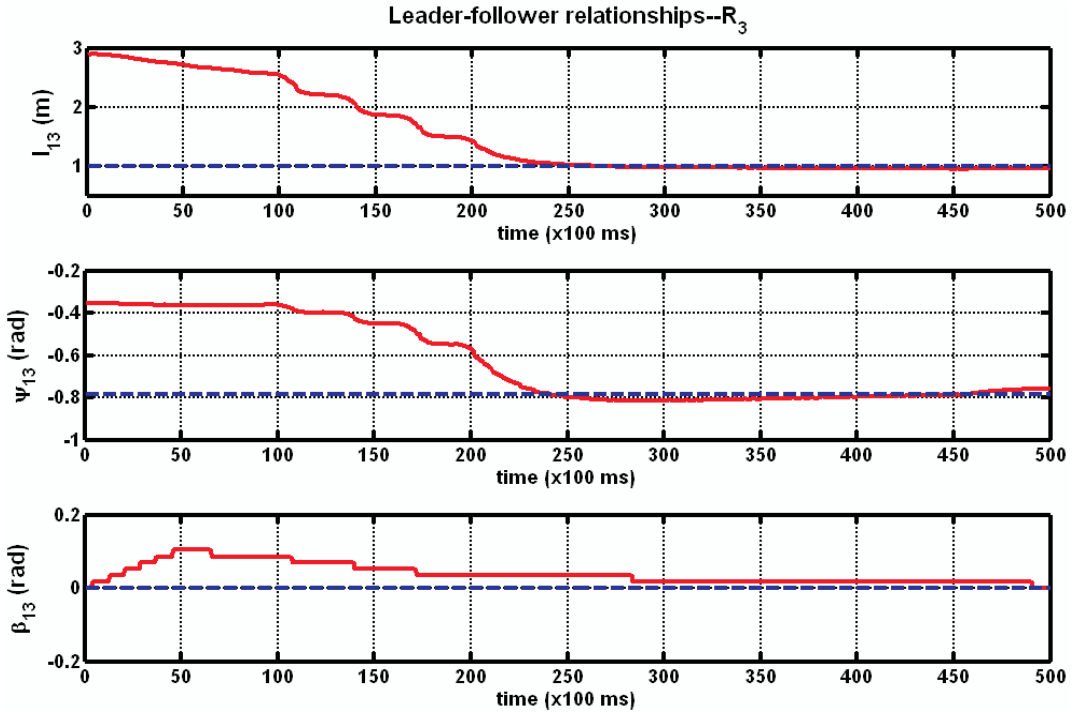


(b)

Fig. 18. Leader–follower relationships of the formation backwards task. (Solid line: Actual. Dashed line: Required.)

## References


Balch, T., and Arkin, R. C. (1998). Behavior-based formation control for multi-robot teams. *IEEE Transactions on Robotics and Automation*, **14**(6): 926–939.

Beard, R. W., Lawton, J. and Hadaegh, F. Y. (2001). A coordination architecture for spacecraft formation control. *IEEE Transactions on Control System Technology*, **9**(6): 777–790.

Berman, S., Edan, Y. and Hamshidi, M. (2004). Navigation of decentralized autonomous automatic guided vehicles in material handling. *IEEE Transactions on Robotics and Automation*, **19**(4): 743–749.

Bloch, A. M., Reyhanoglu, M. and McClamroch, N. H. (1992). Control and stabilization of nonholonomic dynamic systems. *IEEE Transactions on Automatic Control*, **37**(11): 1746–1757.

Brockett, R. W. (1983). Asymptotic stability and feedback stabilization. *Differential Geometric Control Theory*, pp. 181–191.

Burgard, W., Moors, M., Stachniss, C. and Schneider, F. E. (2005). Coordinated multi-robot exploration. *IEEE Transactions on Robotics*, **21**(3): 376–386.

Cao, Z., Tan, M., Li, L., Gu, N. and Wang, S. (2006). Cooperative hunting by distributed mobile robots based on local interaction. *IEEE Transactions on Robotics*, **22**(2): 403–407.

Chen, H. and Allgower, F. (1998). A quasi-infinite horizon nonlinear model predictive control scheme with guaranteed stability. *Automatica*, **34**(10): 1205–1217.

Chen, H. Y., Sun, D. and Yang, J. (2009). Global localization of multirobot formation using ceiling vision SLAM strategy. *Mechatronics*, **19**.

Chen, J., Sun, D. and Yang, J. (2008). A receding-horizon formation tracking controller with leader–follower strategies. *IFAC 2008 World Congress*, Seoul, Korea, pp. 4400–4405.

Chen, Y. and Wang, Z. (2005). Formation control: a review and consideration. *Proceedings IEEE/RSJ International Conference on Intelligent Robots and Systems*, Alberta, Canada, pp. 3181–3186.

Das, K., Fierro, R., Kumar, V., Ostrowski, J. P., Spletzer, J. and Taylor, C. J. (2002). A vision-based formation control framework. *IEEE Transactions on Robotics and Automation*, **18**(5): 813–825.

De Nicolao, G., Magni, L. and Scattolini, R. (1998). Stabilizing receding-horizon control of nonlinear time varying systems. *IEEE Transactions on Automatic Control*, **43**(7): 1030–1036.

Desai, J. P., Kumar, V. and Ostrowski, P. (2001). Modeling and control of formations of nonholonomic mobile robots. *IEEE Transactions on Robotics and Automation*, **17**(6): 905–908.

Egerstedt, M. and Hu, X. (2001). Formation constrained multiagent control. *IEEE Transactions on Robotics and Automation*, **17**(6): 947–951.

Fax, J. A. and Murray, R. M. (2004). Information flow and cooperative control of vehicle formations. *IEEE Transactions on Automatic Control*, **49**(9): 1465–1476.

Fontes, F. A. C. C. (2001). A general framework to design stabilizing nonlinear model predictive controllers. *System and Control Letters*, **42**(2): 127–143.

Gu, D. (2008). A differential game approach to formation control. *IEEE Transactions on Control Systems Technology*, **16**(1): 85–93.

Gu, D. and Hu, H. (2005). A stabilizing receding horizon regulator for nonholonomic mobile robots. *IEEE Transactions on Robotics and Automation*, **21**(5): 1022–1028.

Huang, J., Farritor, S. M., Ala' Qadi and Goddard, S. (2006). Localization and follow-the-leader control of a heterogeneous group of mobile robots. *IEEE/ASME Transactions on Mechatronics*, **11**(2): 205–215.

Jadbabaie, A., Lin, J. and Morse, A. S. (2003). Coordination of groups of mobile autonomous agents using nearest neighbor rules. *IEEE Transactions on Automatic Control*, **48**(6): 988–1001.

Jiang, Z. P. and Nijmeijer, H. (1997). Tracking control of mobile robots: a case study in backstepping. *Automatica*, **33**(7): 1393–1399.

Kanayama, Y., Kimura, Y., Miyazaki, F. and Noguchi, T. (1990). A stable tracking control method for an autonomous mobile robot. *Proceedings IEEE International Conference on Robotics and Automation*, Cincinnati, OH, pp. 384–389.

Keerthi, S. S. and Gilbert, E. G. (1988). Optimal infinite-horizon feedback laws for a general class of constrained discrete-time systems: stability and moving-horizon approximations. *Journal of Optimization Theory and Applications*, **57**(2): 265–293.

Lawton, J. R. T., Beard, R. W. and Young, B. J. (2003). A decentralized approach to formation maneuvers. *IEEE Transactions on Robotics and Automation*, **19**(6): 933–941.

Lewis, M. A. and Tan, Kar-Han (1997). High precision formation control of mobile robots using virtual structures. *Autonomous Robots*, **4**: 387–403.

Liu, J. and Wu, J. (2001). *Multi-agent Robotic Systems*. CRC, Boca Raton, FL.

Long, M., Gage, A., Murphy, R. and Valavanis, K. (2005). Application of the distributed field robot architecture to a simulated Deming task. Proceedings IEEE International Conference on Robotics and Automation, Barcelona, pp. 3204–3211.

Moreau, L. (2005). Stability of multiagent systems with time-dependent communication links. *IEEE Transactions on Automatic Control*, **50**(2): 169–182.

Ogren, P., Fiorelli, E. and Leonard, N. E. (2004). Cooperative control of mobile sensor networks: adaptive gradient climbing in a distributed environment. *IEEE Transactions on Automatic Control*, **40**(8): 1292–1302.

Olfati-Saber, R. (2006). Flocking for multi-agent dynamic systems: algorithms and theory. *IEEE Transactions on Automatic Control*, **51**(3): 401–420.

Olfati-Saber, R. and Murray, R. M. (2004). Consensus problems in networks of agents with switching topology and time-delays. *IEEE Transactions on Automatic Control*, **49**(9): 101–115.

Parker, L. E. (1998). ALLIANCE: an architecture for fault-tolerant multirobot cooperation. *IEEE Transactions on Robotics and Automation*, **14**(2): 220–240.

Rawlings, J. B. and Muske, K. R. (1993). Stability of constrained receding horizon control. *IEEE Transactions on Automatic Control*, **38**(10): 1512–1516.

Ren, W. and Beard, R. W. (2004). Formation feedback control for multiple spacecraft via virtual structures. *IEE Proceedings—Control Theory Application*, **151**(3): 357–368.

Scokaert, P. O. M., Mayne, D. Q. and Rawlings, J. B. (1999). Suboptimal model predictive control (feasibility implies stability). *IEEE Transactions on Automatic Control*, **44**(3): 648–654.

Sepulchre, R., Paley, D. and Leonard, N. E. (2007). Stabilization of planar collective motion: all-to-all communication. *IEEE Transactions on Automatic Control*, **52**(5): 811–824.

Sun, D. and Wang, C. (2007). Controlling swarms of mobile robots for switching between formations using synchronization concept. *IEEE International Conference on Robotics and Automation*, Roma, pp. 2300–2305.

Takahashi, H., Nishi, H. and Ohnishi, K. (2004). Autonomous decentralized control for formation of multiple mobile robots considering ability of robot. *IEEE Transactions on Industrial Electronics*, **51**(6): 1272–1279.

Tang, Z. and Ozguner, U. (2005). Motion planning for multi-target surveillance with mobile sensor agents. *IEEE Transactions on Robotics*, **21**(5): 898–908.

Tanner, H. G., Loizou, S. G. and Kyriakopoulos, K. J. (2003). Nonholonomic navigation and control of multiple mobile manipulators. *IEEE Transactions on Robotics and Automation*, **19**(1): 53–64.

Tanner, H. G., Pappas, G. J. and Kumar, V. (2004). Leader-to-formation stability. *IEEE Transactions on Robotics and Automation*, **20**(3): 443–455.

Yamaguchi, H. (1999). A cooperative hunting behavior by mobile-robot troops. *The International Journal of Robotics Research*, **18**(9): 931–940.

Yamashita, A., Arai, T., Ota, J. and Asama, H. (2003). Motion planning of multiple mobile robots for cooperative manipulation and transportation. *IEEE Transactions on Robotics and Automation*, **19**(2): 223–236.